JOURNAL OF THERMOPHYSICS AND HEAT TRANSFER
Vol. 13, No. 1, January–March 1999

Spectroscopic Measurements of Shock-Layer Flows in an Arcjet Facility

Chung S. Park,* Mark E. Newfield,† Douglas G. Fletcher,‡ and Tahir Gökçen*
NASA Ames Research Center, Moffett Field, California 94035-1000

Under two different test conditions, radiation emanating from the freestream and shock-layer flow over a 15.24-cm-diam blunt-body test article as measured in NASA Ames Research Center's 20 MW Aerodynamic Heating Facility Arcjet. The test gas was a mixture of air and argon. Spatially resolved emission spectra were obtained over a 2000–8900 Å wavelength range using a charge-coupled device camera (1024 × 256 array) attached to a spectrograph. The optical system was calibrated using tungsten and deuterium radiation sources. Previously developed analytical tools were used to determine the following line-of-sight-averaged thermodynamic properties from the calibrated spectra: 1) rotational temperature of the freestream and 2) rotational and vibrational temperatures within the shock layer. Based on the variation in intensity of emission spectra along the stagnation streamline, shock standoff distance was determined. Two sets of data for each test condition were compared to evaluate the repeatability of measurements. Considering likely sources of errors, an uncertainty analysis was performed to estimate the error bounds of the determined properties.

Nomenclature

I = arc current, A
p = pressure, Pa
T = temperature, K
V = arc voltage, V
W = shaded area in Figs. 5 and 6
x = distance from the model surface, mm
σ = standard deviation

Subscripts
e = electronic
r = rotational
sc = settling chamber
tr = translational
v = vibrational

Introduction

ARCJET wind-tunnel facilities produce high-enthalpy hypersonic flows that have been used for purposes as diverse as testing spacecraft thermal-protection materials, investigating catalytic recombination of atoms on surfaces, and simulating combustion in airbreathing engines operating at hypersonic speeds. Owing to this versatility, there is considerable interest in improving the general state of knowledge of arcjet flows.

As part of ongoing investigations into arcjet characterization at the NASA Ames Research Center,[1–3] effort has been directed toward improving our knowledge of these flows through the acquisition and analysis of radiative emission from the freestream and shock-layer flow over a blunt-body test article. Therein, tests were conducted at the highest stagnation pressure in the NASA Ames 20 MW Aerodynamic Heating Facility Arcjet (AHF) and with a large-diameter test model. To extract useful information from the large amount of spectral data and thereby determine the thermodynamic conditions of the freestream and shock-layer flow, several analytical approaches for determining temperatures from radiative emission were tested and implemented. These included methods for obtaining 1) T_r of the freestream using NO γ and δ systems and 2) T_r, T_v, and T_e of the shock layer using the N_2^+ 1− system and oxygen lines. Also, uncertainty analyses of the measured temperatures and number densities of N_2^+, N_2, O, and N were performed.

As a continuation of a previous work,[1] additional tests were conducted at two different conditions: 1) the same condition as in the previous work, and 2) at relatively low pressure, where thermochemical equilibrium is less likely within the shock-layer flow. The methodologies developed in the previous work for determining temperatures were improved, and they were used to analyze time-averaged emission spectra from the freestream and the blunt-body shock layer that were spatially resolved along the stagnation streamline. In addition, T_r of the freestream was compared with that from a concurrent laser-induced fluorescence (LIF) measurement.[4]

To improve the uncertainty estimates, additional sources of uncertainty were included: curve fitting on the spectra, coma, and the light-acceptance cone shaped by the optical arrangements. With these improvements, uncertainty analyses of the measured temperatures were performed to estimate the errors in the determined temperatures. To check the repeatability of the tests, two sets of data were obtained under each test condition. Based on the analysis of the repeatability, the reliability of the determined temperatures was examined.

Experiment

Apparatus

The experiment was conducted in the AHF. A schematic diagram of the facility and experimental setup is shown in Fig. 1. The test gas was heated in a 216-cm-long, 6-cm-diam constrictor section. The constrictor was followed by a 10-cm-long, 10.4-cm-diam electrode package, which serves to a limited extent as a settling chamber. Downstream from the electrode package, the flow was expanded through a converging–diverging conical nozzle. A water-cooled flat-faced cylindrical model of 15.24 cm diameter was used to generated the shock-layer flow.

The arrangement of the optical system is shown in Fig. 2. The optical arrangement was set such that radiation emanating

---

Presented as Paper 98-0893 at the AIAA 36th Aerospace Sciences Meeting, Reno, NV, Jan. 12–15, 1998; received March 30, 1998; revision received July 23, 1998; accepted for publication July 23, 1998.

*Senior Research Scientist, Thermosciences Institute.

†Research Scientist, Reacting Flow Environments Branch.

‡Research Scientist, Reacting Flow Environments Branch. Senior Member AIAA.

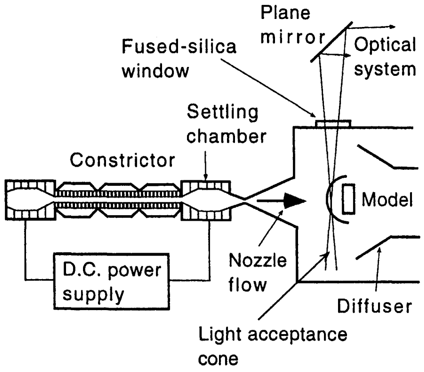

Fig. 1 Schematic of the facility and experimental setup.

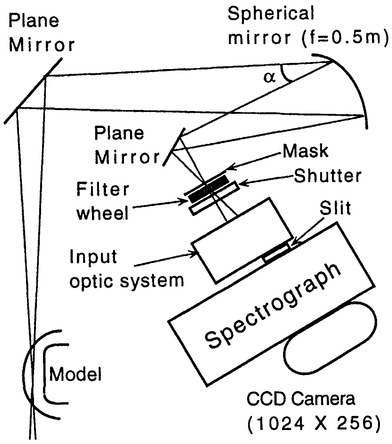

Fig. 2 Arrangement of the optical detection system for the shock-layer emission measurements.

from an object area of 200 × 508 μm was imaged on the detecting surface of a charge-coupled device (CCD) camera at a size of 50 × 127 μm. With the mask segmented into eight distinct apertures, radiation was collected from eight object area locations along the stagnation streamline, with each location separated approximately by 3 mm. The detailed description of the facility, optical arrangement, optical elements, and calibration process can be found in Ref. 1.

Test Conditions

The arc heater was operated at two conditions: 1) $p_{sc} = 6.88 \times 10^5$ Pa, $I = 2075$ A, and $V = 5630$ V, and 2) $p_{sc} = 1.72 \times 10^5$ Pa, $I = 1141$ A, and $V = 2657$ V. In the following sections, the high and low pressure refer to the first and second test condition, respectively. The test gas consisted of air and argon at an unknown mixture ratio. To estimate the mixture ratio, a separate measurement of flow rate was performed, and argon mass flow rate was approximately 5 and 30% for the high- and low-pressure case, respectively.

Measured Spectra

In this section, the emission spectra for the low-pressure case will be shown because the general features of the emission spectra were quite similar for the two cases. Also, the detailed description of emission spectra of the high-pressure case is discussed in Ref. 1.

Freestream

Emission spectra from the freestream were recorded with the model translated out of the flow. The emission spectra were taken at wavelength intervals of 2000–8900 Å, and the only significant radiation emanated from NO in electronically excited states (Fig. 3). The spectrum in Fig. 3 is one of the eight spectra taken simultaneously by the CCD camera. The other seven spectra were identical to that in Fig. 3.

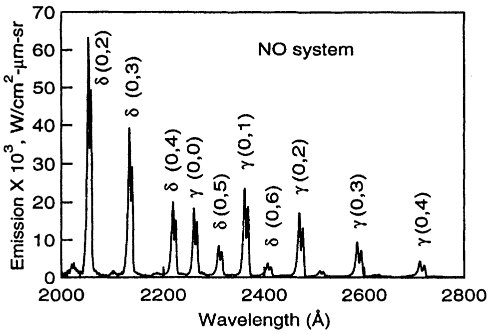

Fig. 3 Freestream spectra acquired 30 cm from the nozzle exit.

As indicated in Fig. 3, the spectral bands detected were identified as the NO γ and δ systems. The NO γ and δ band systems correspond to the $A^2\Sigma^+ - X^2\Pi$ and $C^2\Pi - X^2\Pi$ transitions, respectively. For both systems, only vibrational transitions from the upper level of $v' = 0$ were of sufficient intensity to be recorded during the exposure time. Emission from higher vibrational states was not discernible above the background light level, which is clearly evident between the designated spectral features in the figure.

To measure the contribution of stray light from longer wavelengths to the background signal, a long pass filter (WG-320) was used. This measurement showed that the light level from longer wavelengths was less than 2% of the peak value of the signal, which implied the existence of unidentified band systems in the background signal.

Shock Layer

A complete image of the shock-layer flow was obtained by positioning the water-cooled copper model at two locations in two separate facility runs: 34.5 and 36.9 cm downstream from the nozzle exit and recording complete sets of spectral data for each location. At each location of the model, eight spectra were recorded simultaneously for each grating position of the spectrograph.

In Figs. 4a–4c, emission spectra taken at various wavelength intervals, at a location 17.9 mm from the model surface, are shown. (To reduce the number of figures, some of the separately acquired spectra are merged into a longer region where clarity is not compromised.) In the 2000–3000 Å range, as shown in Fig. 4a, NO γ was the most significant system. Further analysis on the NO spectra will be reported in the following sections.

In the 3300–4300 Å range, as shown in Fig. 4b, the identified transitions were attributed to the N_2 2+, N_2^+ 1−, and CN Violet systems. In Fig. 4c, the dominant emission features are O and N atomic lines, with a broad background contribution from the N_2 1+ system emission. At spatial locations closer to the model surface, which are not shown, the N-atom emission level was not much greater than the N_2 1+ emission that underlies it. This made it impractical to attempt to extract information from the N-atom emission, despite the large number of recorded multiplet signals.

Data Analysis

In this section, analytical approaches to determine the rotational and vibrational temperatures and uncertainties of these values are presented. For the shock-layer flow, additional sources of uncertainty are considered. Also, based on the absolute intensity values of several spectral features, the shock standoff distances are determined.

Freestream

Temperatures

The rotational temperature T_r was determined from the well-resolved vibrational bands in Fig. 3. The full width of the

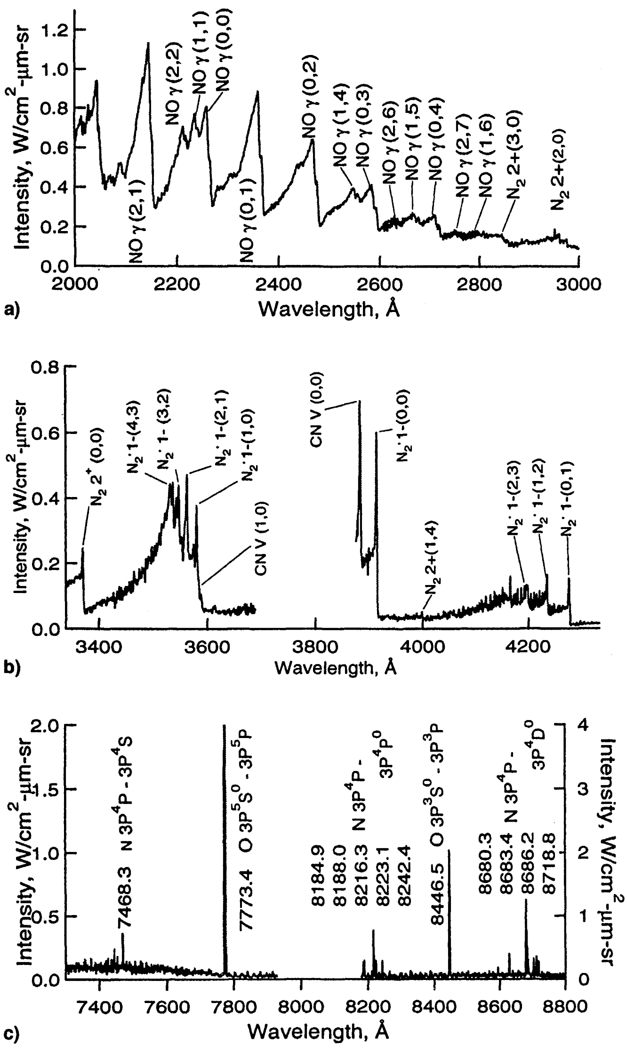

Fig. 4 Spectral emission emanating from the shock layer around a flat-faced cylindrical model of 15.24 cm in diameter. The spectra were acquired 17.9 mm away from the model surface. Emission spectra in the a) 2000–3000 (NO β system underlies), b) 3500–4300, and c) 7300–8800 Å ranges.

half maximum (FWHM) of the band intensity was calculated for a number of cases and correlated with T_r. The correlation between T_r and the FWHM was developed using the NEQAIR code.[5] NEQAIR generates synthetic spectra by calculating all of the atomic lines and molecular band systems line-by-line and by adding all of the lines. As in the previous study,[1] five bands were used to read T_r: NOδ(0,4), γ(0,0), γ(0,1), γ(0,2), and γ(0,3). For each band system, a correlation was established. Then, each measured FWHM of the NO γ band from the spectra in Fig. 3 was applied to the correlation to determine T_r. A more detailed description on the correlation curves can be found in Ref. 1.

To determine the vibrational temperature, T_v, of NO, emission from two different upper vibrational levels was needed. As only bands from $v' = 0$ state were observed in the spectra, T_v values for NO could not be determined. Instead, the upper limit on T_v could be determined because higher vibrational bands disappear at low T_v. Taking T_v as a parameter and assuming a Boltzmann distribution of population among the vibrational levels, synthetic spectra were generated by NEQAIR until $v' > 0$ bands appeared in the synthetic spectra. The threshold for the appearance of these bands was 950 K, which provided the upper limit of T_v for both the high- and low-pressure cases.

Uncertainty in Temperatures

As is evident in Fig. 3, the background signal directly affected the maximum value of each band system. The error resulting from this background signal was estimated following the same approach as in the previous work.[1] A synthetic spectrum was generated, using the determined T_r value (and $T_v \leq 950$ K). The difference between the synthetic spectrum and experimental data, after adjusting the synthetic peak value to match the experiment, was taken as the unresolved background signal. The standard deviation of this background signal level adjacent to each band system was calculated and then used as an estimate of the uncertainty in the maximum value of the band system signal. The error in T_r was estimated based on the effect of this uncertainty on the FWHM for each band system.

Shock Layer

Temperatures

As shown in Fig. 4b, the N_2^+ 1− band system was the most dominant and it proved to be the most reliable for determining line-of-sight- (LOS-) averaged values of T_r and T_v.[1] In previous work, several methods for determining T_r and T_v from N_2^+ emission spectra were evaluated.[1] Therein, the best approach was to use the ratio of integrals over the wavelength in certain regions. Ratios of the integrals were correlated with T_r and T_v using NEQAIR. Then the ratios obtained from the measured spectra were used to determine T_r and T_v, based on the correlations.

In Fig. 5, the intervals 1 and 2 of the N_2^+ 1− (0,0) band system are shown by the extent of the shaded region that represents the actual areas used in the determination of T_r. As indicated in Fig. 5, the area baseline was taken from the minimum near the bandhead rather than the absolute zero of the spectral intensity, to reduce the contribution of any unresolved background light to the integrals.

T_v from N_2^+ 1− system emission was deduced using an approach similar to that used in the T_r evaluation. In Fig. 6, what

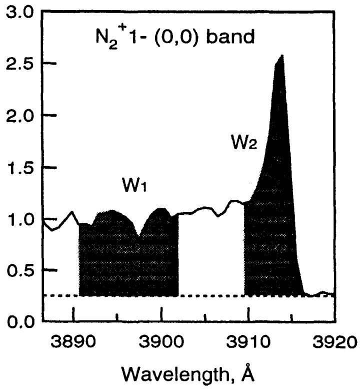

Fig. 5 Pair of spectral integrals used in T_r determination.

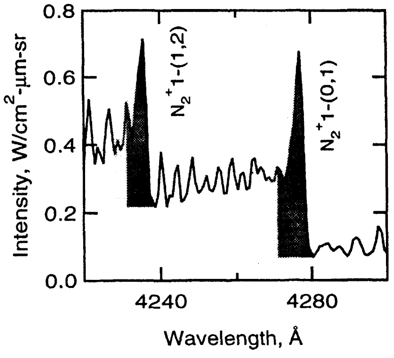

Fig. 6 Pair of spectral integrals used in T_v determination.

were determined to be the optimum intervals for this application are shown by the extent of the shaded region. As can be seen in Fig. 6, intervals for the area ratio were taken from two band systems of different upper-state vibrational quantum numbers. Also, the intervals were taken near the bandheads to maximize signal levels and permit easy identification. To reduce the contribution of the background signal, each area was measured from the minimum near the bandhead, as shown in Fig. 6.

Integration of the areas for experimental spectra in Figs. 5 and 6 was affected by the resolution of the data. This was because of the discrete nature of the wavelength value of experimental data, as seen in Fig. 5. To minimize the effects of finite resolution, cubic-spline curve fitting was performed on the experimental data before the areas in Figs. 5 and 6 were integrated. The curve fitting improved the accuracy in the determination of wavelength, which consequently improved the accuracy of the integration of the areas in Figs. 5 and 6.

Uncertainty in Temperatures

As found in a previous work,[1] the uncertainty in T_r was mainly a result of the background signal that is thought to consist of stray light and contributions from unidentified species. The same approach was used in the current study to estimate the error caused by the background signal. A synthetic background spectrum was generated by using the determined temperatures to generate an emission spectrum with NEQAIR, which was then subtracted from the measured spectrum after adjusting the peak heights to match. The integration of this synthetic background spectrum over the fixed wavelength bandwidths in Figs. 5 and 6 was calculated as a function of wavelength. The standard deviation of the integrated background signal was then taken as representative of the uncertainty in the areas. Based on the analysis in Ref. 6, the standard deviation of T_r, σ_{T_r}, was calculated as

$$\sigma_{T_r} = \sqrt{\left(\frac{\partial T_r}{\partial W_1}\sigma_{W_1}\right)^2 + \left(\frac{\partial T_r}{\partial W_2}\sigma_{W_2}\right)^2} \tag{1}$$

where W_1 and W_2 represent the shaded areas in Fig. 5, and σ_{W_1} (or σ_{W_2}) represents the standard deviation of W_1 (or W_2) because of the background signal. As mentioned, the correlation between T_r and W_1/W_2 was established to determine T_r. Using this correlation and Eq. (1), σ_{T_r} was estimated. Because ratios of spectral features from a single vibrational band were used to determine the rotational temperatures, it is expected that uncertainties in the calibration of the spectral intensities and uncertainties in relative transition strength factors will be negligible compared with the contribution from the unresolved background signal. To estimate the error in T_v, an analysis similar to that of T_r was performed.

As mentioned earlier, to determine the background contribution to the error in temperatures, the spectra from known species were subtracted from the experimental data. In a previous study,[1] those species were N_2 and CN. However, further investigation revealed that the NO β system could have some effect on the determination of temperature, owing to the long red-degraded tail of NO β.

To analyze the thermal status of NO, synthetic NO spectra were generated with an assumption that the population distribution among the electronic states follows a Boltzmann distribution. The electronic temperature was assumed to be the same as T_v. The comparison of the synthetic spectra with the experimental data in Fig. 4a showed a large discrepancy, and indicated that the Boltzmann assumption for NO electronic states is not valid in both high- and low-pressure cases.

Even though further analysis on the mechanisms of NO excitation was not done, efforts were made to estimate the spectral intensity of the NO β system in the range of 3800–4300 Å, based on the signal at a shorter wavelength. Firstly, using the spectral features of the NO γ system at the 2300–2600 Å range, the intensity of the NO γ system near 2800 Å was determined. Because the signal near 2800 Å in Fig. 4a is mainly because of the NO γ and β system, the intensity of the NO β system could be determined by subtracting the NO γ spectrum from the experimental data.

Additional Sources of Uncertainty

In addition to the background signal, likely sources of uncertainty in T_r and T_v were considered in the current study. In the following sections, the effects of the sources on the determination of temperatures are discussed.

Effect of Curve Fitting to Temperatures

As mentioned, cubic-spline curve fitting was performed on the experimental spectra before the areas in Figs. 5 and 6 were integrated. Because the curve-fitting process can be a source of error, its effect on the temperature reading was estimated. As a first step of the estimation, a high-resolution synthetic spectrum at a given set of T_r and T_v was generated by the NEQAIR code. Then, an artificial spectrum with the same resolution as the CCD array was generated from the synthetic spectrum so that the resolution of the experimental data could be simulated. The analysis in previous sections were performed on the artificial spectrum to obtain T_r and T_v. The difference between the obtained temperatures and the given ones at the first step was assumed to be the possible error caused by the finite resolution.

Coma

Another source of uncertainty originated from the coma of the spherical mirrors in the spectrograph. The spectrograph used in the measurement was a Czerny–Turner, which consists of two concave spherical mirrors and one planar diffraction grating. This type of plane grating system (PGS) exhibits certain aberrations such as astigmatism, coma, spherical aberration, and defocusing.[7]

In the current work, the effect of coma on the temperature was considered. As mentioned, eight spectra were captured simultaneously for each grating position of the spectrograph, i.e., each spectra was captured using a different portion of the CCD array. The effect of coma is to shift the spectra in the wavelength direction as a portion of the CCD array is off center of the optical axis. In Fig. 7, the eight spectra of the N_2^+ $1-$ (0,0) band system taken simultaneously under the high-pressure condition are shown. The location of the peak changes from the top to the bottom of the CCD array.

To calculate the effect of shifting on the values of temperatures, a synthetic spectrum with high resolution was generated at a given set of T_r and T_v as a first step. Then, five spectra

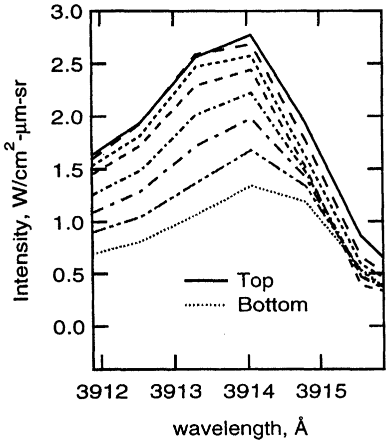

Fig. 7 Eight spectra of N_2^+ 1 − (0,0) band taken simultaneously, showing the wavelength shifting of spectral features because of coma.

with the same resolution as the CCD array were obtained from the synthetic spectra, while each of the five spectra was shifted by 0.2 pixel. The techniques in the previous section were applied to read T_r and T_v for the spectra, which yielded five sets of T_r and T_v. Using these values and the measured shifting of wavelength, the temperature deviation because of coma can be calculated. Also, the standard deviation of five sets of temperature deviation was taken as the indicator of the uncertainty because of the coma.

Spatial Resolution

As shown in Fig. 2, the optical system was designed to image object areas along the stagnation streamline onto the mask. If only the gas near the stagnation streamline was emitting, the spatial resolution in the two orthogonal directions normal to the optical axis would be 508 and 200 μm. However, the optical system collected photons from emitting gas particles in the light acceptance volume as well as those from gas particles within the object area.

In Fig. 8, one of the eight light-acceptance volumes is sketched with a coordinate system. Therein, the x and z axis represent the direction of stagnation streamline and LOS, respectively. The dimensions of the planar area of the acceptance volume, Δx and Δy, were calculated using ray-tracing software[8] and are shown in Ref. 1.

The dimensions of the cone are not small compared with the shock standoff distance, which will be mentioned in the following section. This attribute of the light-collection geometry degrades the spatial resolution and causes an averaging of flow gradients because the measurement locations partially overlap near the shock front region.

Because the size of the light-acceptance cone was fixed during the measurements, it was not possible to determine experimentally the effect of the contribution from the emitting gas particles in the light-acceptance volume to the temperatures.

Instead, the results from numerical simulations[2,9] of the flowfield were used in the estimation of the effect. In Refs. 2 and 9, numerical simulations of the temperatures and species number densities in the flow were performed for the high- and low-pressure test conditions. The flow properties along the centerline and four corners of the light-acceptance cone in Fig. 8 were obtained from the numerical simulation. Using these flow properties, LOS spectra from each corner and centerline were generated and temperatures were determined from the spectra. The difference between temperatures from each corner and the centerline could be considered as the indicator of uncertainty because of light collection geometry, i.e., degraded spatial resolution.

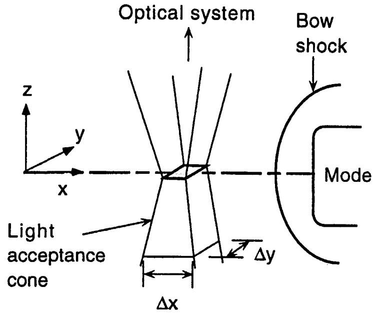

Fig. 8 Schematic of the light-collecting cone.

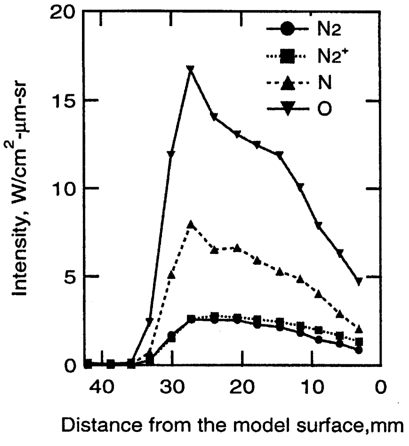

Fig. 9 Spectral intensity at four wavelengths as functions of distance from the model surface for the high-pressure condition.

Shock Standoff Distance

As mentioned earlier, the spectra were scanned at 16 locations along the stagnation streamline. The radiation front could be determined by plotting the spectral intensity variation along the 16 locations. Because it is possible that the shock wave is not located where the radiation front is, the direct measurement of the shock standoff distance was not possible. In the following sections, the shock standoff distance actually represents the distance between the model surface and the radiation front.

In Fig. 9, the spectral intensities at four wavelengths for one of the two tests for the high-pressure case are plotted as functions of the distance from the model surface. Therein, the x axis represents the distance between the model surface and each location along the stagnation streamline. The four wavelengths were selected to represent the major species: N_2^+ 1− (0,0) bandhead, N_2 2+ (0,0) bandhead, 8446.5 Å for O atoms, and 8680.3 Å for N atoms. In Fig. 9, the signal level starts increasing 33.2 mm from the model surface. Because the neighboring location in the upstream side is located 35.8 mm from the model, the shock standoff distance was 34.5 ± 1.3 mm, based on the radiation measurement.

For the low-pressure case, the same analysis was performed and the distance based on the atomic species was 37.3 ± 1.5 mm, whereas the distance based on the molecular radiation was the same as the high-pressure case.

Results

LOS-averaged values of T_r and T_v were determined from the measured emission spectra using the approaches outlined earlier. Uncertainties for each determined quantity were also calculated considering the contributions from several sources of uncertainty. Using one of the methodologies in a previous work[1] as an independent technique, the T_v values were determined and compared.

Freestream

Five different NO bands were used to determine T_r in the freestream and the temperatures determined from these bands are shown in Table 1, along with the uncertainties for each determination. As mentioned, two sets of data were obtained for both high- and low-pressure cases. Thus, T_r values of each column in Table 1 represent the average of 32 data points.

For each band system, T_r was determined from eight separate spatial measurements and these values did not show any

Table 1 Determined T_r for each band system of NO[a]

	δ(0,4)	γ(0,0)	γ(0,1)	γ(0,2)	γ(0,3)
		High-pressure case			
T_r	860	904	985	991	992
σ	57	98	71	74	58
		Low-pressure case			
T_r	604	572	628	616	609
σ	35	55	36	35	38

[a] σ is the uncertainty because of the background signal and random errors. The values are in units of K.

systematic trend in both the high- and low-pressure cases. Thus, the measurements could be considered as eight independent measurements rather than a single sample measurement at eight locations. Also, as two sets of tests were performed for each test condition, $32T_r$ values were available for each band system. The standard deviation of the $32T_r$ values was determined from each band system. This standard deviation was combined with that resulting from the background, and it is shown in Table 1. As seen in Table 1, the error bound of T_r value from each band system overlaps with those from the other band systems.

A concurrent measurement of translational temperature T_{tr} of the freestream was performed using the LIF technique. A description of the method for determining T_{tr} is given in Ref. 4. This independent measurement showed that T_{tr} of the freestream was 1640 ± 400 K and 820 ± 250 K for the high- and low-pressure cases, respectively. Under the current test conditions, the values of T_r and T_{tr} should be close to each other. For the low-pressure case, the values from the two different techniques overlap within their error bounds. However, for the high-pressure case, the values show a difference of several hundred degrees. The source of the discrepancy is not well understood at this point. However, it is possible that the discrepancy might be because of the LOS effect. LIF technique measures the flow on the centerline of the nozzle, whereas the NO-based T_r is integrated along the LOS.

Shock Layer

Temperature

Temperatures (T_r and T_v) were determined for each axial position along the stagnation streamline for the shock-layer flow over the test model using the spectral analysis approaches discussed earlier. Again, the determined values represent the LOS-averaged flow temperatures. The temperatures in high- and low-pressure cases were plotted as functions of distance from the model along the stagnation streamline and are shown in Figs. 10a and 10b. In each figure, two sets of data under the same condition are shown, and the subscripts 1 and 2 of each curve represent the test number. Although the temperatures were all measured at the same location, the values are offset slightly from each other to improve clarity. Error bars for each temperature are used to indicate uncertainties. Therein, the error bars were determined by adding in quadrature the standard deviations of the uncertainties mentioned in the previous section. The uncertainties because of the curve-fitting and coma were comparable to that resulting from the background signal, whereas the effect of the spatial resolution was about one-third of that resulting from the background signal.

In Fig. 10b, the T_v values near the shock wave show large error bars, which are mainly because of the background signal. The error bound of T_v at the location of $x = 33.2$ mm was so large that T_v at that location was not shown in the figure. The reliability of the determined temperatures in Figs. 10a and 10b will be discussed further in the Discussion section.

As in a previous work,[1] electronic temperatures were determined using the ratio of intensities from the two strong O atom lines at 7773 and 8446 Å. However, the results are not presented in this paper because of the large uncertainty. As seen in Fig. 4c, there exists a fair amount of background signal near the oxygen lines. To subtract the background signal, a Gaussian curve fitting was used. Depending on the offset of the baseline in curve fitting, the value of electronic temperature showed a large variation. It is mainly a result of the high sensitivity of electronic temperature to the change of the intensity ratio of atomic lines at 7773 and 8446 Å. To obtain an electronic temperature with less uncertainty, atomic line spectra with a larger energy difference in the upper states are needed. Measurements of the atomic lines in the range of 9000–10,500 Å are underway.

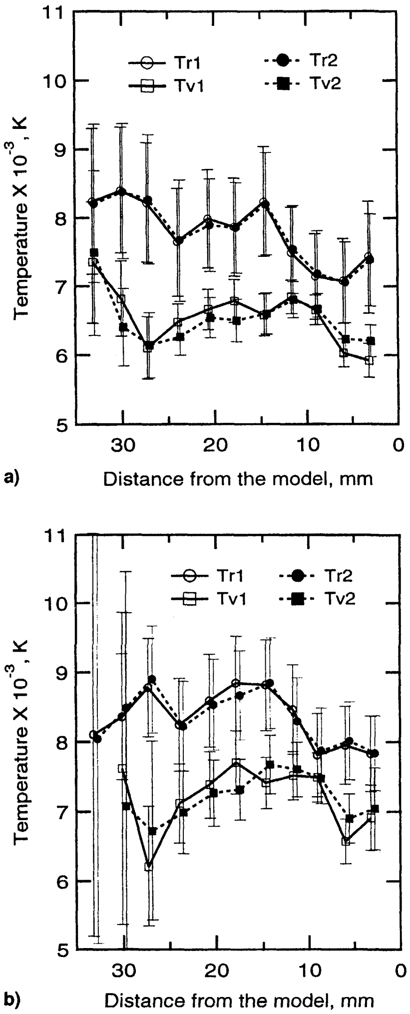

Fig. 10 Temperatures as functions of the distance from the model surface for the a) high- and b) low-pressure condition. Numbers in each curve represent the test number.

Number Densities

Once the LOS-averaged temperatures were determined, they were used to derive the LOS-averaged species number densities by again invoking the assumption that the electronic state populations follow a Boltzmann distribution and the T_e is the same as T_v. However, it should be kept in mind that all temperatures in the previous sections were determined based on the emission spectra. Thus, the obtained temperatures represent population distributions of the excited electronic states. For the temperature range in Figs. 10a and 10b, the number density in electronically excited states was quite small compared with that of the ground states for all species. Consequently, the thermal status of the excited states may not represent that of the total flow.

The determined number densities showed relatively large error bounds. These arise from the exponential dependence of number density on temperature. As an example, the error bound of the number densities because of the electronic temperature uncertainty was calculated at 11.9 mm from the model surface in the high-pressure case. The N_2^+, N_2, O, and N number density showed a change by factor of 1.58, 4.9, 4.9, and 5.5, respectively. Thus, other strategies are needed for obtaining information about the number densities.

T_v Using Peak Ratio Method

In the previous study,[1] the ratios of signal peaks at bandheads were used to determine T_v for the high-pressure case. Therein, the peak ratio methods were shown to be inferior to

Table 2 T_v **and the uncertainty of** T_v **for the two tests under the low-pressure case**[a]

	Test no. 1				Test no. 2			
	Area ratio		Peak ratio		Area ratio		Peak ratio	
x, mm	T_v	σ_{T_v}	T_v	σ_{T_v}	T_v	σ_{T_v}	T_v	σ_{T_v}
30.10	7617	2251	6310	2353	7075	3380	6784	3481
27.31	6211	868	6620	928	6725	1289	6880	1396
23.98	7116	563	6500	639	6989	593	6560	668
20.70	7386	477	7192	544	7266	471	7166	539
17.86	7706	456	7210	577	7317	435	7292	561
14.63	7408	368	7520	415	7672	422	7500	463
11.68	7515	347	7160	389	7601	390	7250	428
9.04	7488	352	7080	430	7469	359	7208	436
5.97	6573	320	7160	416	6897	350	7458	440
3.20	6908	464	7300	529	7042	585	7792	638

[a] Area ratio represents the ratio of areas in Fig. 6, whereas the peak ratio represents the ratio of peaks between N_2^+ 1− (2,1) and (0,0) bandhead. Temperatures are in K.

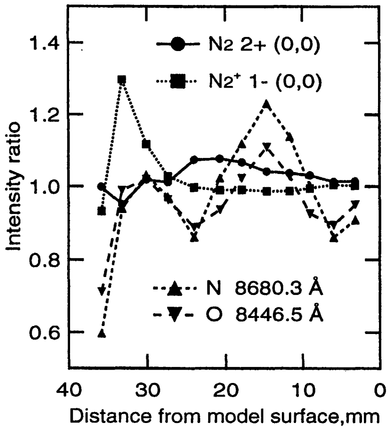

Fig. 11 Ratio of intensities from the two tests at four wavelengths as functions of distance from the model surface for the high-pressure condition.

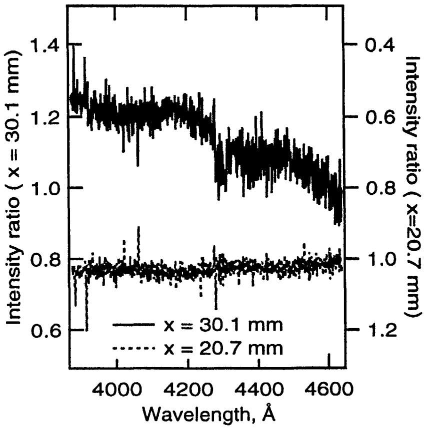

Fig. 12 Ratio of intensities from the two tests as a function of wavelength for the high-pressure condition. The spectra were taken at two locations: 30.1 and 20.7 mm from the model surface.

the area ratio method for several reasons. However, as an independent methodology, the peak ratio method can be used to check the validity of the temperatures in Figs. 10a and 10b. In the current study, the N_2^+ 1− (2,1) and (0,0) peak ratio was also used to determine T_v. As in the previous study, to reduce the contribution of background signal, the peak was measured from the minimum near the bandhead, as shown in Fig. 5. In Table 2, the determined T_v for the low-pressure case are listed.

In Table 2, the area ratio represents the methodology mentioned in previous sections; i.e., the T_v values of these columns are the same as those in Fig. 10b. The test numbers represent the numbers in the curves in Fig. 10b. The T_v values from two different methods overlap within their error bounds.

Discussion

Repeatability

In Fig. 9, the spectral intensities at four wavelengths for the high-pressure case were plotted as functions of the distance from the model surface. The four wavelengths were selected to represent the major species: N_2^+, N_2, O, and N atoms. Because two sets of measurements were performed for each test condition, the intensity ratios between the two sets of emission spectra at four selected wavelengths could be indicators of the repeatability of the measurements. These ratios determined at the 11 locations along the stagnation streamline are shown in Fig. 11 for the high-pressure case. As seen, only N_2^+ showed relatively good repeatability at nine locations from the model surface for the high-pressure case. For the low-pressure case, the plot of intensity ratio shows a similar trend as in Fig. 11 and, therefore, is not shown here. The plot for the low-pressure case can be found in Ref. 3.

In Fig. 11, the intensity ratios of N_2^+ have large scatter at the first few locations behind the shock wave. It could be naturally expected that the scatter in the ratios are largest near the shock front, where radiation is developing, i.e., signal levels are low. Also, the other species show a larger scatter in the entire shock-layer regime than that of N_2^+. It was speculated that the scatter could be a result of the fluctuation of the shock standoff distance as well as possible small changes of operational conditions of the facility during the test. The fluctuation of the radiation front could be observed visually during the experiments. The operational conditions could not be exactly repeated for the two tests under one condition, even though an attempt was made to run the tests under the same condition. In this study, no assessment of the effects of the changes in the operational condition to the scatter in the Fig. 11 has been made.

As seen in Fig. 11, the atomic species have a larger scatter than that of N_2^+. One of the possible explanations for this larger scatter is the shorter integration time for the atomic spectra. Because the fluctuation is a function of time, the spectra taken at a shorter integration time are more likely affected by the fluctuation than those at a longer integration time. To improve the repeatability of atomic spectra, a longer integration time with a neutral density filter is currently used in ongoing measurements. The effects of the fluctuation on the repeatability will be analyzed in the following study.

Because the N_2^+ 1− system was mainly used in the temperature determination, the intensity ratio of spectra in the wavelength range of 3900–4600 Å was also analyzed. In Fig. 12, the intensity ratios at two locations, 30.1 and 20.7 mm from the model surface, are plotted as functions of wavelength. Therein, the spectra of the two tests under the high-pressure condition were used in the ratio. There is a variation in ratio at 30.1 mm from the model surface. The magnitude of this variation increases as the intensity ratio of N_2^+ in Fig. 11 deviates more from 1.0. The variation of ratio as a function of wavelength would affect the temperature values because the temperatures were determined by taking the ratio of areas at selected wavelength intervals, as shown in Figs. 5 and 6. Thus, the temperatures determined near the shock wave would show a larger scatter than those near the model surface for repeated experiments. A sensitivity analysis in a previous study[1] showed that 5% variation in the ratio of areas in Figs. 5 and 6 would result in a 2000 and 400 K difference in T_r and T_v, respectively. As a consequence, the reliability of the determined temperatures at the locations where the intensity ratio of N_2^+ was more than a few percent off from 1.0 was questionable. In the following discussion, the temperatures at such locations were not considered.

Similar analysis was performed on the spectra in the wavelength range of 2600–3400 Å, even though the ratio plot is omitted for simplicity. The ratio plot shows that the ratio deviates from 1.0 near the bandheads of the N_2 2+ system by 10%. Thus, it can be concluded that temperatures determined from the N_2 2+ system would show a larger statistical uncertainty than those from the N_2^+ 1− system, unless the background is carefully subtracted from the experimental data for these measurements.

NO Spectra

As mentioned earlier, the NO β spectra was considered in the analysis of T_r and T_v of the shock layer. In the high-pressure case, the measured intensity of the NO β system was one order of magnitude smaller than that of the numerical simulation. In the numerical simulation, the Boltzmann assumption was used to calculate the populations in the electronic-excited states. In the low-pressure case, the NO β system was not present in the spectra. From these observations and similar observations of freestream spectra, it was concluded that the electronic states of NO are not in Boltzmann equilibrium for all conditions of these tests. Because the exact mechanisms of the electronic excitation of NO under the conditions of the current study are not known, further analysis is needed.

Temperatures

As can be seen in Figs. 10a and 10b, T_r was systematically higher than T_v along the stagnation streamline. It was speculated that this difference could be caused by a strong signal contribution from the flow region near the shock-front radiation, which may be in thermal nonequilibrium, to the total emission recorded along the LOS. As the experimental data were only acquired at one set of spanwise locations along the stagnation streamline, there was not sufficient information to perform an Abel transformation. Consequently, only properties of the nonuniform flow that were spatially averaged along the optical path could be determined from this experimental data. Thus, instead of mapping out the flow properties point-by-point for comparison with computations, comparisons were limited to LOS-averaged properties and emission spectra that were calculated using NEQAIR with flow properties from a numerical solution in Refs. 2 and 9, more detailed analyses based on these comparisons were performed to determine the flow characteristics. A set of off-centerline measurements are underway to determine the LOS effects on the temperature.

Summary

Spectroscopic measurements were conducted in the 20 MW AHF Arcjet Facility at NASA Ames Research Center using a CCD camera capable of recording radiation from eight locations along a stagnation streamline. The spectra from the shock-layer flow around a model and freestream were taken for the investigation of flow characteristics: temperatures and number densities. The wavelengths of the molecular band systems and atomic lines were used to identify the species present in the flow. The identified species were N_2, N_2^+, CN, NO, N, and O.

LOS-averaged values of T_r for the freestream, and T_r and T_v in the shock layer, were determined using ratios of spectral emission integrals over certain wavelength regions. Possible sources of uncertainty in temperatures were considered and their effects were included in the determination of the total uncertainty. The rotational temperature of freestream was compared with the translational temperature derived from LIF measurements. The results of the analysis on T_e and number density were not presented because of large uncertainties.

Based on the absolute intensity ratio of two separate tests under the same test condition, repeatability of the measurements was evaluated and assessments were made of the reliability of the extracted temperatures.

One of the essential characteristics of arcjet facilities is the flow enthalpy. Even though the temperatures were determined at a known stagnation pressure, the point-by-point mapping of the flow enthalpy directly from the experimental data was not possible because of the finite size of the light acceptance cone, flow nonuniformity, and the possible nonequilibrium phenomena of the flow. Instead, comparisons between calculated spectra based on the numerical simulation and the measured spectra in current work were performed in Refs. 2 and 9 for the high- and low-pressure cases, respectively. Therein, based on these comparisons, inferences about the thermochemical state of the shock-layer flow are drawn and discussed.

Acknowledgment

C. S. Park and T. Gökçen acknowledge support from the Reacting Flow Environments Branch at NASA Ames Research Center through Contract NAS2-14031 to Eloret.

References

[1] Park, C. S., Newfield, M. E., Fletcher, D. G., Gökçen, T., and Sharma, S. P., "Spectroscopic Emission Measurements Within the Blunt-Body Shock Layer in an Arc-Jet Flow," *Journal of Thermophysics and Heat Transfer*, Vol. 12, No. 2, 1998, pp. 190–197.

[2] Gökçen, T., Park, C. S., Newfield, M. E., and Fletcher, D. G., "Computational Simulation of Emission Spectra from Shock Layer Flows in an Arc-Jet Facility," *Journal of Thermophysics and Heat Transfer*, Vol. 12, No. 2, 1998, pp. 180–189.

[3] Park, C. S., Newfield, M. E., Fletcher, D. G., and Gökçen, T., "Spectroscopic Measurements of the Flows in an Arc-Jet Facility," AIAA Paper 98-0893, Jan. 1998.

[4] Fletcher, D. G., "Arcjet Flow Properties Determined from Laser-Induced Fluorescence of Atomic Nitrogen," AIAA Paper 98-0205, Jan. 1998.

[5] Park, C., "Nonequilibrium Air Radiation (NEQAIR) Program: User's Manual," NASA TM 86707, July 1985.

[6] Kline, S. J., and McClintock, F. A., "Uncertainties in Single-Sample Experiments," *Mechanical Engineering*, Vol. 75, No. 1, 1953, pp. 3–8.

[7] Möller, K. D., "Coma," *Optics*, 1st ed., University Science Books, Mill Valley, CA, 1988, pp. 444–447.

[8] "BEAM 4 Optical Ray Tracer," Stellar Software, Berkeley, CA, 1994.

[9] Gökçen, T., Park, C. S., and Newfield, M. E., "Computational Analysis of Shock Layer Emission Measurements in an Arc-Jet Facility," AIAA Paper 98-0891, Jan. 1998.